INTERNATIONAL JOURNAL OF HYDROGEN ENERGY 40 (2015) 9013–9025

Available online at www.sciencedirect.com

ScienceDirect

journal homepage: www.elsevier.com/locate/he

Decentralized power and heat derived from an eco-innovative integrated gasification fuel cell combined cycle fuelled by waste

Tygue S. Doyle [a,*], *Zahir Dehouche* [a], *Sinisa Stankovic* [b]

[a] *Centre for Energy and Built Environment Research, Brunel University, London UB8 3PH, UK*
[b] *ChapmanBDSP, Saffron House, 6-10 Kirby Street, London EC1N 8TS, UK*

ARTICLE INFO

Article history:
Received 19 February 2015
Received in revised form
15 May 2015
Accepted 22 May 2015
Available online 19 June 2015

Keywords:
Waste-to-energy
Gasification
Fuel cells
Electrolysis
Hydrogen storage
Decentralised CHP

ABSTRACT

The suitability for fuel cells to run on synthesis gas coming from the gasification of waste is determined by the sensitivity of the fuel cell to run on contaminated fuel. Out of the available fuel cell technologies solid oxide fuel cells (SOFCs), because of their ceramic construction and high operating temperatures, are best suited for syngas operation. Their high operating temperature (>650 °C) and the presence of nickel at the anode means that it is possible to reform hydrocarbons to provide further hydrogen [1].

Numerical simulations representing all aspects of the proposed system have been developed to understand the energy performance of the system as a whole as well as the financial and environmental benefits. Taking into account variations in the waste composition and the wholesale electricity price the proposed system, scaled to process 100,000 tonnes of waste per year (40,000 removed for recycling), has a simple payback period of 7.2 years whilst providing CO_2 savings of 13%. Over the year the proposed system will provide enough electricity to supply more than 23,000 homes and enough heat for more than 5800 homes.

Copyright © 2015, The Authors. Published by Elsevier Ltd on behalf of Hydrogen Energy Publications, LLC. This is an open access article under the CC BY-NC-ND license (http://creativecommons.org/licenses/by-nc-nd/4.0/).

Introduction

Escalating energy demands, energy security issues and the current political drive to reduce carbon emissions have created an overwhelming need for innovative and future-proof decentralised energy production and management solutions to tackle the area of sustainable energy production. Over the past century there has been an exponential growth in energy consumption of which 80% is derived from fossil fuels [2]. Current estimations see coal as the only fossil fuel to be available after 2042 and will only be available up to 2112 [3]. At the same time there is growing concern surround the emission of greenhouse gasses which contribute to global warming disrupting the current climate rhythm.

This has led to substantial interest and deployment of solar powered renewable technologies such as wind turbines, photovoltaics (PV), and biomass. As an energy resource the potential for wind energy in the UK is very strong and is considered to the best wind resource in Europe [4]. Whilst wind turbines and PVs are fundamentally sustainable with relatively short energy payback periods they are inherently

* *Corresponding author*.
E-mail address: Tygue.Doyle@brunel.ac.uk (T.S. Doyle).
http://dx.doi.org/10.1016/j.ijhydene.2015.05.151
0360-3199/Copyright © 2015, The Authors. Published by Elsevier Ltd on behalf of Hydrogen Energy Publications, LLC. This is an open access article under the CC BY-NC-ND license (http://creativecommons.org/licenses/by-nc-nd/4.0/).

intermittent which means the electricity grid will struggle to support their deployment at large scale. Therefore, further technologies dealing with the dynamic relationship between demand and supply will be required to support the large-scale penetration of any intermittent energy sources.

There is also a need for effective and sustainable waste management at a time when households are producing ever more waste. In some cases this waste is sent to large centralised waste incinerators which are unable to make full use of the waste heat (which is >65% of the total energy content) and therefore unable to fully re-capture the embodied energy. They also have disadvantages in terms of emissions and solid by-products which are often classified as hazardous.

In order to maximise efficiency and to bring these waste-to-energy (WtE) systems closer to the end users – where waste heat can be utilised in intelligent building-to-building thermal energy networks – new technologies must be introduced [1].

Currently only 20% of the municipal waste produced in Europe is sent to incineration plants [5], and of the waste generated in the UK it is estimated that 40% is considered to be bio-waste [6,7]. Therefore there is a large potential to provide carbon emissions savings by diverting waste away from landfill to WtE plants that can efficiently recover the embodied energy within the waste to produce energy. The biofraction of the waste stream is considered as a renewable source of energy thereby providing carbon savings.

The waste, hydrogen, heat and electricity (WHHE) concept

This concept and research relies on the successful integration of proven cutting-edge fuel processing, energy production and energy storage technology in a new and innovative manner to achieve a highly efficient and flexible decentralized energy system for the building industry. These technologies include: thermal plasma gasification, gas filtering, hybrid fuel cell/heat engine combined cycle, hydrogen production (electrolysis), hydrogen storage (nanostructured high capacity metal hydrides), enhanced heat exchange and effective thermal management systems, Fig. 1. This system represents an ambitious step in the direction of energy decarbonisation and security by providing decentralised clean and efficient energy centres for the long term, comprehensive management of heat, electricity, hydrogen and waste.

Modelling theory and methodology

In this research Simulink®, which is an interactive graphical block programming tool that integrates with MatLab®, is used to carry out selective modelling of several of the energy processes (Fig. 2). The algorithms used to describe the various processes are based on static and dynamic equations that are either derived from experimental results or obtained through literature.

For those processes where Simulink modelling is not best suited ChemCad has been used. ChemCad is ideally suited to modelling of the chemical processes such as gasification, gas filtration and separation, and heat management.

SOFC modelling

Due to the complexity and importance of the SOFC the modelling goes into details which are well suited to the functionality and capabilities of Simulink's modelling environment.

The performance of the SOFC is defined by the Nernst equations which describes the reversible voltage as a function of the partial pressure of product (H_2O) and the reactants (H_2, O_2):

$$E = E^{o} + \frac{RT}{nF} ln\left[\left(\frac{p_{H_2}}{p_{H_2O}}\right)\left(\frac{p_{O_2}}{p_0}\right)^{1/2}\right]$$

Therefore, in order to accurately simulate the interaction of the various gases, introduced via the syngas composition, mass transport calculations are carried out for Knudsen, ordinary and effective diffusion coefficients which are applied to the Maxwell–Stefan diffusion model for binary mixtures. The Maxwell–Stefan model is then manipulated to calculate the partial pressures to be used in the Nernst equation [8]:

$$p^{*}_{H_2} = p_{ch,H_2} - \frac{jRTt_a}{2FD_{H_2,H_2O}};$$

$$p^{*}_{H_2O} = p_{ch,H_2O} + \frac{jRTt_a}{2FD_{H_2,H_2O}};$$

$$p^{*}_{O_2} = P_{ch,c} - \left(P_{ch,c} - p_{ch,O_2}\right)\exp\left(\frac{jRTt_c}{4FP_{ch,c}D_{O_2,N_2}}\right)$$

Losses at the fuel cell come from; activation losses (activation energy required to overcome the charge double layer), concentration losses (restricted transportation of reactants and products to/from the reaction site), and ohmic losses (losses due to resistance – imperfect conduction).

Activation losses are calculated using the cell's current density and exchange current density:

$$\eta_{act} = \frac{RT}{\alpha nF}\log\left(\frac{j}{j_0}\right)$$

Where the exchange current density is calculated according to the Arrhenius law – which is again a function of the partial pressures of the product and reactants at the anode and cathode [9]:

$$j_{0,a} = \gamma_{an}\left(\frac{p_{H_2}}{P_{ref}}\right)\left(\frac{p_{H_2O}}{P_{ref}}\right)\exp\left(-\frac{E_{act,a}}{RT}\right)$$

$$j_{0,c} = \gamma_{cat}\left(\frac{p_{O_2}}{P_{ref}}\right)^{0.25}\exp\left(-\frac{E_{act,c}}{RT}\right)$$

Concentration losses are most noticeable at high current densities where the cell is starved from insufficient reactants reaching the reaction site and where the product is struggling to move away from the reaction site. Therefore by manipulating the Nernst equation the concentration losses can be defined by a limiting current density [10]:

$$\eta_{conc} = \frac{RT}{nF}\ln\frac{j_L}{j_L - j}$$

where

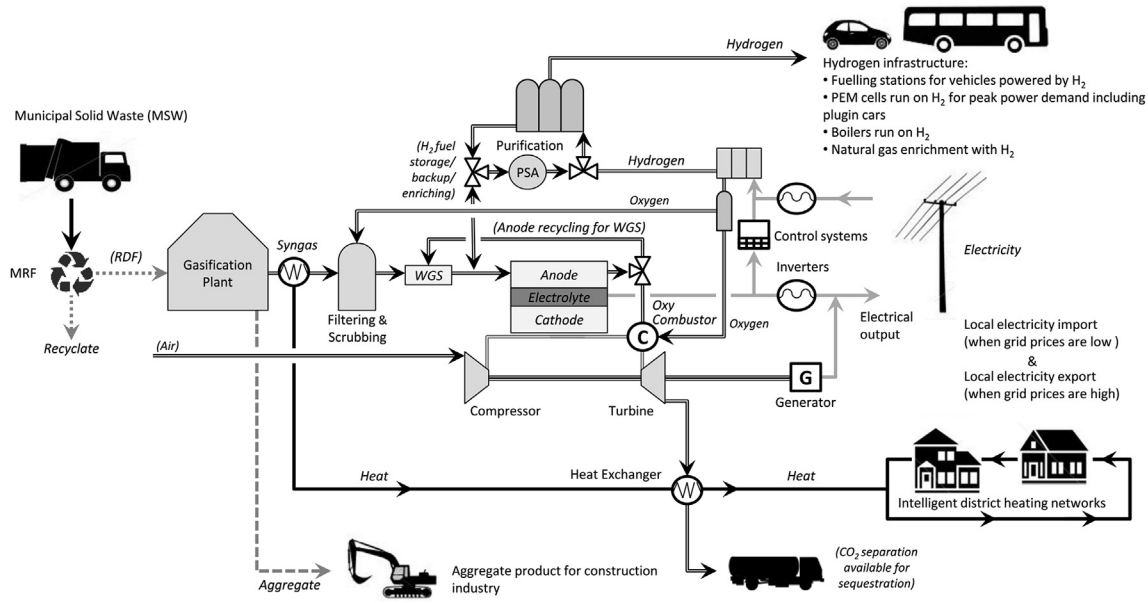

Fig. 1 – Schematic of a Dual fluidised bed/plasma gasification, hydrogen storage, SOFC/GT hybrid system.

$$j_L = nFD_{ij,eff}\frac{c_R^0}{t}$$

Lastly, ohmic losses are dependent on geometry which is why the fuel cell's resistance is often normalised by area and known as the area-specific resistance (ASR):

$$\eta_{ohmic} = j(ASR_{ohmic})$$

where

$$ASR = \frac{t}{\sigma}$$

and

$$\sigma T = A_{SOFC}e^{-\Delta G_{act}/RT}$$

$$A_{sofc} = c(zF)^2 D_O/R$$

Heat transfer within the fuel cell is carried out by means of; convection, radiation and mass flow. Based on the conservation of energy the heat is generated from the electrochemical reaction and the total heat balance can be defined as [8]:

$$\dot{q}_{in} = \dot{q}_{gen} = \dot{q}_{chem} - \dot{q}_{elec}$$

$$\dot{q}_{out} = \dot{q}_{rad} + \dot{q}_{conv} + \dot{q}_{flow}$$

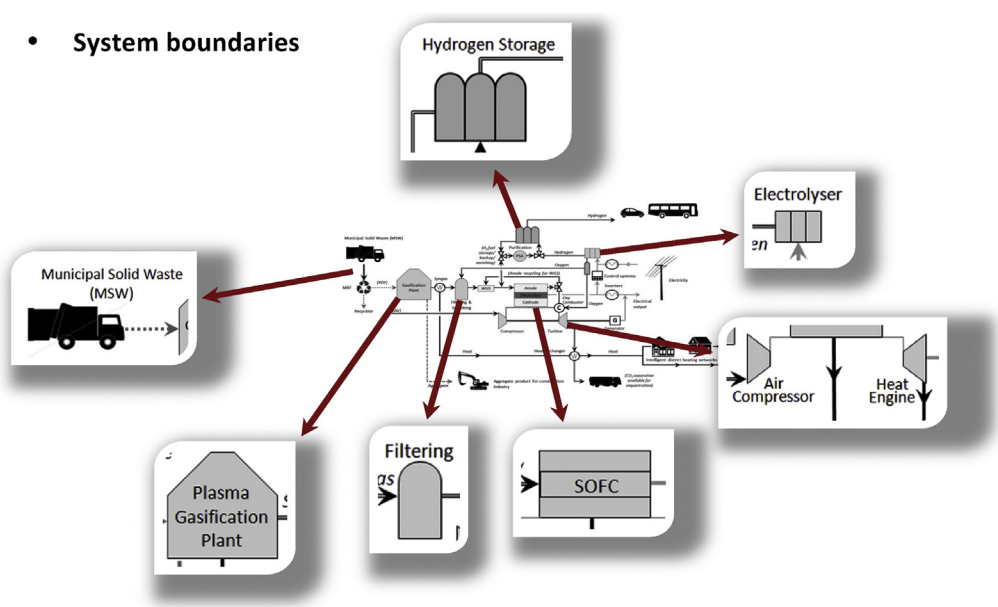

Fig. 2 – Highlighting of system boundaries identified for modelling.

$$\therefore \dot{q}_{net} = \dot{q}_{in} - \dot{q}_{out} = m_{cell} c_{cell} \frac{dT_{cell}}{dt}$$

where

$$\dot{q}_{chem} = \dot{n}_{H_2,consumed}.\Delta H$$

$$\dot{q}_{elec} = V_{out}.i$$

$$\dot{q}_{rad} = \varepsilon\sigma A(T_{hot}^4 - T_{cold}^4)$$

$$\dot{q}_{conv} = hA(T_{hot} - T_{cold})$$

$$\dot{q}_{flow} = \sum_i \dot{n}_i C_{p,i} \left(\frac{dT}{dt}\right)$$

Gas turbine

Gas turbine (GT) theory and modelling is very mature so derivation into Simulink is straight forward. Fig. 3 illustrates how the GT is implemented making use of heat from the fuel cell to charge the compressed air coming from the compressor via a heat exchanger.

The thermodynamic expression for the change in temperature for a given pressure ratio and isentropic efficiency is given by:

$$T_{02} - T_{01} = \frac{T_{01}}{\eta_c}\left[\left(\frac{p_{02}}{p_{01}}\right)^{(\gamma-1)/\gamma} - 1\right]$$

Where γ is the ratio of specific heats for the fluid – in this case air.

Similarly for the turbine:

$$T_{03} - T_{04} = \eta_t T_{03}\left[1 - \left(\frac{1}{p_{03}/p_{04}}\right)^{(\gamma-1)/\gamma}\right]$$

The power generated after the energy required to drive the compressor is deducted using:

$$\therefore \dot{W}_{net} = \dot{W}_{tur} - \dot{W}_{com}$$

$$\Rightarrow \dot{W} = \dot{m} c_p \Delta T$$

Electrolyser

Electrolysis is the function of a fuel cell working in reverse. By passing a current between two electrodes separated by an electrolyte we are able to decompose water into its elementary components H_2 and O_2.

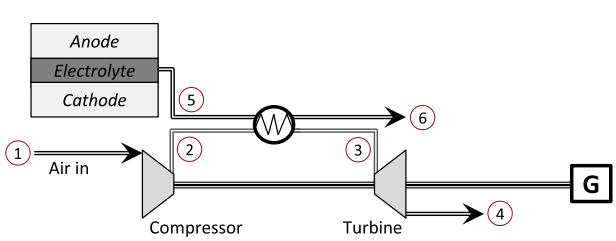

Fig. 3 – Unpressurised SOFC-GT hybrid configuration.

According to Faraday's law the production of hydrogen is directly proportional to the amount of current provided [11,12]:

$$\dot{n}_{H_2} = \eta_F \frac{i_e}{2F}$$

Where η_F is the Faraday efficiency which is the ratio between the theoretical and actual maximum amount of hydrogen produced by the electrolyser, and i_e is the electrolyser current (A). The Faraday efficiency (η_F) can be derived as [11,12]:

$$\eta_F = \frac{j^2}{f_1 + j^2} f_2$$

Where j is the current density (A/m^2), and f_1 and f_2 are coefficients derived from experimental results and vary linearly with temperature (Table 1) [13].

Hydrogen storage

The potential to store hydrogen in solid state hydrogen storage containers commonly uses hydride materials consisting of binary, ternary, or quaternary hydride compounds. The reaction of hydrogen with these metallic compounds involves changes in enthalpy with absorption being exothermic and desorption endothermic. The change in free energy in a gas compressed isothermally can be expressed as:

$$\Delta G = RT \ln \frac{p}{p_0}$$

When considering the various materials available the materials used in current commercial applications are magnesium based (MgH_2). MgH_2 presents advantages of high storage capacity by weight (7.6% H-wt% [14]), and materials are abundant and cheap. However, disadvantages are that magnesium based materials have slow sorption kinetics and high thermodynamic stability ranges therefore requiring higher temperatures for desorption. The high temperatures required for desorption is not a major factor for this research as there is an abundant supply of high grade heat (>350 °C) supplied by both the GT and fuel cell. Therefore, the application of magnesium based hydrogen storage is well suited. The storage capacity will be limited by the amount of heat available above the operating temperature for desorption, but must be large enough to cover scheduled maintenance of the gasifier. Absorption can be carried out at ambient conditions but because of the exothermic nature of the reaction energy for cooling will be required to maintain the absorption kinetics. Therefore, in order to identify the amount of heat required to be removed and provided during absorption and desorption the enthalpy of formation is required. Typical values of the reaction enthalpy for MgH_2 is 37.5 kJ/(mol H_2) [15,16] 1). Absorption takes place at 2 bar and 30 °C and

Table 1 – Faraday efficiency coefficients (Ulleberg, 2003).

T	40	60	80
f_1	150	200	250
f_2	0.990	0.985	0.980

desorption will take place at atmospheric pressure and 320 °C. Fig. 4 illustrates the absorption and desorption characteristics of Mg-based nanocomposite (MgH_2-3 at%V-2at.%Ti) material prepared by high energy ball milling and operating at 300 °C and discharge near atmospheric pressure. Fig. 4 also shows that magnesium based metal hydrides show favourable energy densities when compared to other metal hydrides [17].

From this information the heat transfer to and from the hydrogen unit can be calculated via:

Isolating the required mass flow results in:

$$\text{For cooling} \quad \dot{m}_{air} = \frac{\dot{m}_{H_2} 37.5 \times 10^3}{C_{p_{air}}(303 - T_{amb})}$$

$$\text{For heating} \quad \dot{m}_{hot} = \frac{\dot{m}_{H_2} 37.5 \times 10^3}{C_{p_{hot}}(T_{hot} - 593)}$$

Oxy combustor

The exhaust gas leaving the fuel cell will still contain unutilised fuel in the form of H_2 and CO. So, in order to capture this remaining energy a combustion chamber is used to oxidise the remaining fuel; thereby increasing the turbine inlet temperature.

It must be assumed that the combustion is complete, therefore having a complete conversion of H_2 to H_2O, and CO to CO_2, enabling the calculation of molar quantities after combustion. The simplest method of calculating the adiabatic flame temperature is to use a constant average C_p [18]:

$$T_P \approx T_R + \frac{-Q^0_{rxn,p}}{\sum_i n_{i,P} C_{pi}}$$

where

$$-Q^0_{rxn,p} = \sum_i n_{i,R} \Delta \hat{h}^0_{i,R} - \sum_i n_{i,P} \Delta \hat{h}^0_{i,P}$$

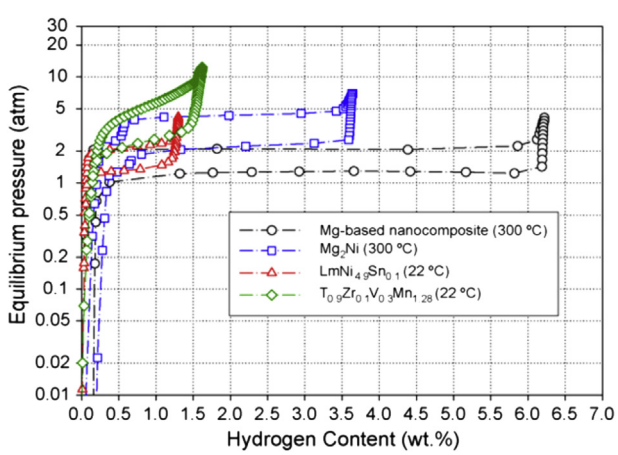

Fig. 4 – Pressure-composition isotherms of different types of metal hydrides showing Mg-based nanocomposites offer higher energy densities at lower pressures [17].

$$Q = mC_p\Delta T$$

Gasification

Using ChemCAD to model gasification equilibrium reactions are calculated by Gibbs free energy minimisation using a GIBs UnitOp. The equation calculating the change in Gibbs free energy where the equilibrium constant is used is known as the van't Hoff isotherm:

$$\Delta G = -RT \ln K_e$$

ΔG is used to measure how far a given reaction is away from equilibrium. If ΔG is large and negative the reaction is spontaneous, and far from equilibrium. Therefore only when ΔG=0 will a position of equilibrium be found.

Calculations for gasification are based on thermodynamics, mass and energy flow, operating conditions (temperature and pressure), and the addition or subtraction of indirect heat. Therefore in order simulate the gasification of municipal solid waste (MSW) the ultimate analysis of the feedstock is required. For MSW the following information has been found in literature (Table 2):

Gasification operation

As mentioned previously, the gasifier has a number of variables to consider during operation all of which have an effect on the performance of the gasifier and the quality of the syngas produced. The most important aspects to look at are:

Stoichiometric oxygen ratio (λ):

$$\lambda = \frac{external\ \ O_2\ supply/fuel\ supply}{stoichiometric\ O_2\ requirement/unit\ of\ fuel\ input}$$

Steam-to-biomass ratio (SB):

$$SB = \frac{steam\ mass\ flow}{fuel\ feed\ flow}$$

Modified steam-to-biomass ratio (SB*):

$$SB^* = \frac{steam\ mass\ flow + fuel\ moisture\ mass\ flow}{dry,\ ash - free\ fuel\ feed\ flow}$$

Energy conversion efficiency (ECE):

Table 2 – Ultimate analysis of various sources of MSW within the UK (where HHV is not available LHV is provided and identified in bold).

	MSW [19]	MSW [20]	RDF [20]	MSW [21]	MSW [22]	RDF [23]
Ultimate analysis, wt%						
C	24.0%	22.2%	54.5%	22.1%	43.0%	28.3%
H	3.2%	3.2%	7.6%	3.2%	5.6%	4.2%
O	15.9%	14.2%	20.5%	14.2%	26.6%	24.3%
N	0.7%	0.6%	0.7%	0.6%	0.6%	0.6%
S	0.1%	0.1%	0.2%	0.1%	0.3%	0.3%
Cl	0.7%	0.6%	0.8%	0.6%	0.3%	0.0%
Si (Ash)	24.2%	27.8%	11.7%	27.8%	12.1%	11.6%
Moisture	31.2%	31.4%	4.1%	31.4%	11.5%	30.7%
HHV/**LHV**	**10.6**	9.4	23.5	9.39	21.0 **(dry)**	11.17

$$ECE = \frac{net\ energy\ content\ of\ the\ syngas\ [MW]}{net\ energy\ content\ of\ the\ input\ fuel\ [MW]}$$

Carbon conversion efficiency (CCE):

$$CCE = \left(1 - \frac{carbon\ content\ of\ residue\ [kmol/h]}{carbon\ content\ of\ input\ fuel\ [kmol/h]}\right)$$

The stoichiometric oxygen ratio (also called equivalence ratio) is used to identify different oxidation approaches as $\lambda = 1$ refers to combustion, $\lambda = 0$ refers to pyrolysis, and $0 < \lambda < 1$ represents gasification. Exothermic oxidation is also used to control the operating temperature of the reactor so whilst very low λ values will generate high yields of hydrogen and carbon monoxide greater levels of oxygen are required to maintain the required operating temperature to sustain the gasification process. Typical λ values used in fluidised bed gasification vary between 0.2 and 0.4 [24,25].

Although the most common fluidisation/moderator and oxidation medium used for gasification is air high levels of nitrogen within the product gas will significantly lower the heating value of the gas. Therefore it is more beneficial to use a combination of oxygen and steam as steam can contribute to the quality of the syngas.

This leads to the significance of knowing the moisture content and to expand to the modified steam-to-biomass ratio (SB*) as controlling the potential steam content will influence the carbon conversion efficiency, energy conversion efficiency, and heating value of the syngas (values for SB between 0.3 and 1.0 have shown to have a positive effect on these factors) [25].

The plasma converter is modelled by assuming a fixed operating temperature which is required to breakdown the tar contaminants. The electrical power required to maintain the thermal plasma reactor temperature is derived from literature [26].

Gas filtering and processing

The modelling of the gas filtering and processing encompasses the air separation unit (ASU), ceramic hot gas filtering using sodium bicarbonate, high temperature and low temperature shift reactions, and desulphurisation using Selexol™.

Air separation unit

Although the plant will benefit from a supply of pure oxygen from the electrolyser the ASU will have to be scaled to meet peak demand in order to cover periods where the electrolyser will not be operating. Because the proposed system is not technically sensitive to the inclusion of nitrogen, and because the size of the plant is relatively small, oxygen purification has been modelled using PSA theory.

Hot gas filtering

To simulate the influence of sodium bicarbonate in the ceramic gas filtering process an equilibrium reactor is used to simulate the following reactions:

$$NaHCO_3 + HCl \rightarrow NaCl + H_2O + CO_2$$

$$2NaHCO_3 + SO_2 + \frac{1}{2}O_2 \rightarrow Na_2SO_4 + 2CO_2 + H_2O$$

The syngas from the gasifier must be cooled before entering the hot gas filtration unit so a heat exchanger is used to control the inlet temperature using air, this air will be used at the inlet to the fuel cell cathode. To simulate the removal of the solid build-up on the filters a solid separation unit is used to remove the salts formed.

High and low temperature shift reactions

Simulation of the high and low temperature shift reactions is carried out using predefined shift equlibrium reactors where reactions are allowed to be carried out adiabatically. The purpose of using two reactors at high and low temperatures is to maximise the hydrogen yield by using various catalysts which are sensitive to temperature [27]. The cooling fluid used to recover and control the temperatures before and after the various reactors is water. Water is inlet to both shift reactors but in the case of the high temperature reactor a heat exchanger is used as a steam generator for the incoming water which serves to control the reactor temperature. Conversely water is directly fed into the low temperature reactor in order to keep the reactor temperature down.

Desulphurisation

Simulation of Selexol™ adsorption is carried out using a standard distillation column operating at elevated pressures and near ambient temperatures. The syngas is compressed and cooled before entering the bottom of the adsorption tower. The filtered syngas then exits from the top of the column where the gas is flashed back to ambient temperature. The Selexol™, rich in H_2S, CO_2 and some COS, is pumped from the adsorption column to a secondary column for regeneration where contaminants desorb from the Selexol™. Regeneration is carried out at a lower pressure and higher temperature than adsorption. The lean Selexol™ is then recycled back to the adsorption column to continue the cycle.

The recovered H_2S, CO_2 and COS can then be sent to a Claus reactor to produce elemental sulphur from the contaminants.

Fuel dynamics

The composition of waste is never fixed and understanding these variations can be very important for waste management planning. There is a number of factors that contribute to these variations and they include; seasonal variations, different regional areas, cultural and ethnic diversity, socio–economic profile, urban context and many other factors that influence consumer trends [28–30].

To take this into account the variation of the waste composition (and subsequent syngas) variations have been added to the results obtained from ChemCad. For simplification variations are made every 24 h and as seen in Fig. 5 the

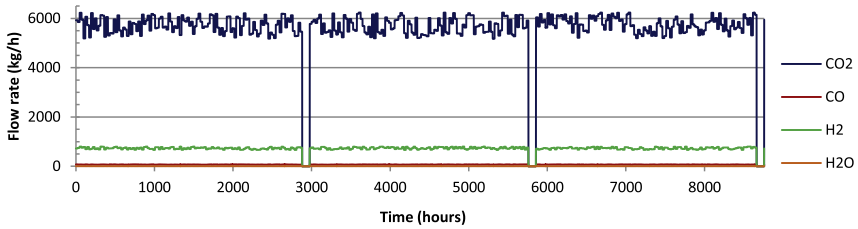

Fig. 5 – Variations in syngas composition including three 4 day maintenance periods.

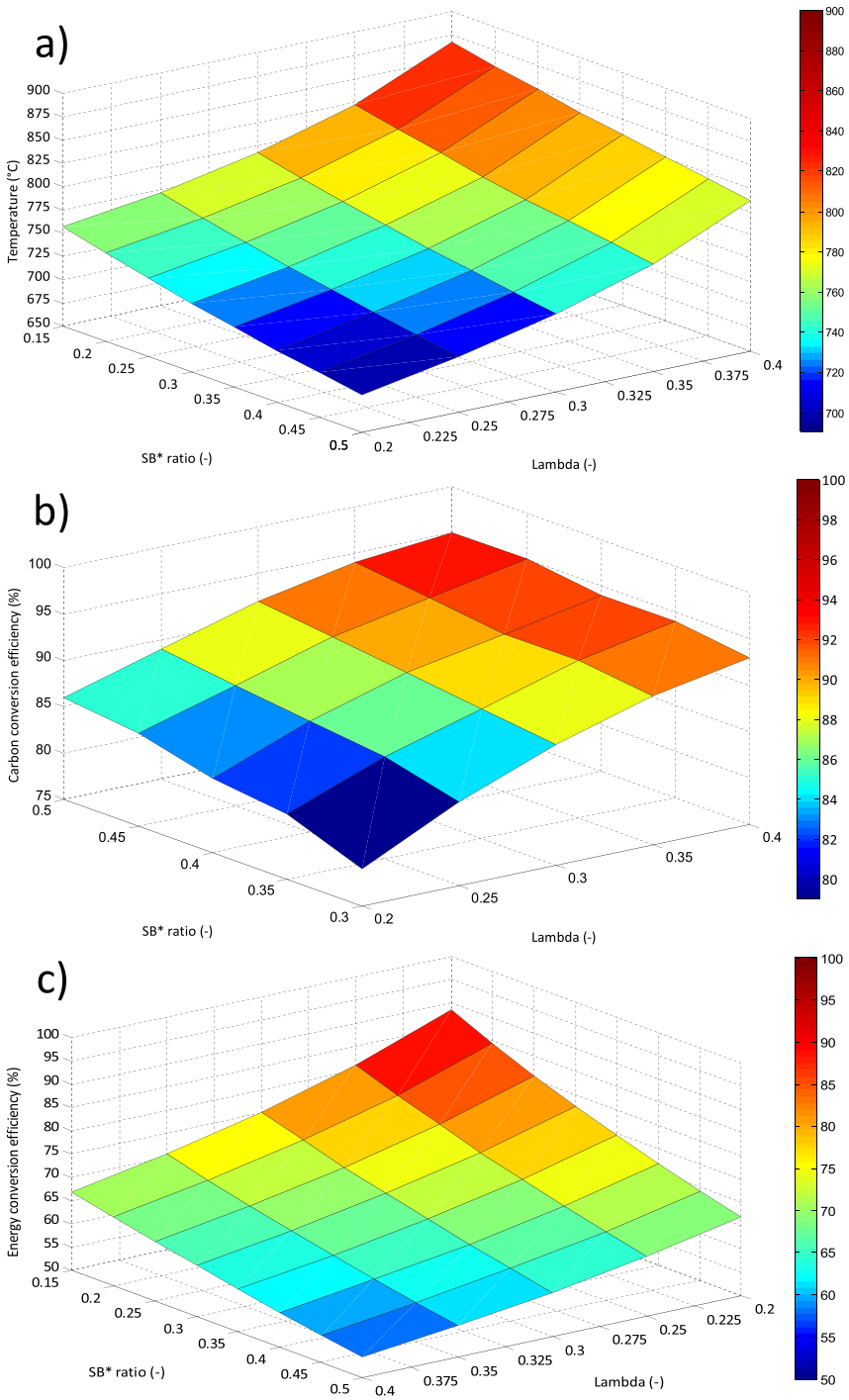

Fig. 6 – 3D surface plot showing a) temperature according to λ and SB*, b) the CCE according to λ and SB* when operating at 850 °C, and c) ECE according to λ and SB*.

Table 3 – Molar % of syngas coming from the gasifier at 816 °C.

Heating values (60 F)	
Gross kJ/kg	1.1E+04
Net kJ/kg	9644
Component mole %	
Hydrogen	38.833
Methane	0.038
Carbon monoxide	31.395
Carbon dioxide	12.924
Water	16.077
Oxygen	0.000
Nitrogen	0.325
Benzene	0.000
Toluene	0.000
Hydrogen chloride	0.147
Sulphur dioxide	0.000
Nitrogen dioxide	0.000
Hydrogen sulfide	0.117

scheduled maintenance periods over the year have been simulated using three 4 day breaks of no fuel.

The operating strategy also calls for a reliable supply of hydrogen to the fuel cell meaning an upper and lower limit must be set for the amount of hydrogen sent to the fuel cell. The excess hydrogen above the upper threshold must then be sent for storage whilst deficiencies must be buoyed by hydrogen coming from storage. This includes maintenance periods where the hydrogen storage must provide the minimum required amount of hydrogen to keep the fuel cell operational (i.e. to prevent the fuel cell from cooling).

Results

The WHHE Energy Centre is sized to handle 100,000 tonnes/year of MSW, of which 40% will be recycled with the remaining 60% converted to RDF. Outputs from the centre will be; electricity, hydrogen, inert slag (aggregate), NaCl (kitchen salt), Na_2SO_4 (sodium salt used as detergent filler), H_2S and COS (and finally elemental sulphur), CO_2 (available for sequestration), hot air (for the fuel cell), and hot water (<100 °C) to be used in district heating.

Table 4 – Composition of the syngas entering and exiting the desulphurisation cycle showing the reduction in contaminants.

Compound	Syngas in	Syngas out	Reduction (%)
	kg/h	kg/h	
H_2	737.216	731.379	0.8%
CH_4	0.0036	0.0033	8.3%
CO	73.142	71.509	2.2%
CO_2	10143.836	5708.770	43.7%
H_2O	1215.622	2.906	99.8%
O_2	0.0088	0.0084	4.5%
N_2	699.184	683.568	2.2%
HCl	0.0819	0.0354	56.8%
H_2S	20.826	0.901	95.7%
COS	1.761	0.0271	98.5%
NH_3	0.026	0.000	100.0%

Gasification and filtration

By plotting temperature, carbon conversion efficiency and energy conversion efficiency as a function of SB* and λ using 3-D surface plots (Fig. 6) it is possible to select a moisture level and oxygen flow rate that can provide syngas at the required quality and efficiency.

As a result the selected values for λ and SB* are 0.35 and 0.2 respectively producing the following syngas composition at 816 °C [Table 3]:

The inert slag being produced at a rate of 929 kg/h is quenched in water where heat is captured through a heat exchanger and serves to supply the water demands of the high and low temperature shift reactors before being exported via the district heating network.

Before the syngas can be filtered through the ceramic hot gas filtration unit it must be cooled to c.a. 450 °C, and because of the high grade heat (>1100 °C) available this is an excellent opportunity to preheat the air required by the fuel cell. At the

Table 5 – Review of ChemCad simulation results.

MSW feedrate	6849	kg/h
MSW LHV	15.7	MJ/kg
Lambda	0.35	(–)
SB*	0.2	(–)
Gasifier temperature	814	°C
ECE	61.4	%
CCE	76.9	%
Plasma T	1200	°C
Hot gas filtering T	345	°C
Sodium bicarbonate in kg/h	71.44	kg/h
Sodium chloride out kg/h	45.052	kg/h
Sodium sulphate out kg/h	0.155	kg/h
High temperature shift inlet T	482	°C
Low temperature shift inlet T	140	°C
Desulphurisation pressure	40	Bar
Desulphurisation T	14.7	°C
Regeneration P	1	Bar
Regeneration T	150	°C
CO_2 out	4435.09	kg/h
H_2S out	19.92	kg/h
COS out	1.73	kg/h
H_2O out	1212.72	kg/h
Heat recovery		
Water flow rate (@86 °C)	7320	kg/h
Air flow rate	24,000	kg/h
Purified syngas composition		
Total flow rate	6976	kg/h
Ultimate analysis	wt %	
H_2	10.16%	
CH_4	0.00%	
CO	0.99%	
CO_2	79.30%	
H_2O	0.04%	
O_2	0.00%	
N_2	9.50%	
C_6H_6	0.00%	
HCl	0.00%	
SO_2	0.00%	
NO_2	0.00%	
H_2S	0.01%	
NH_3	0.00%	

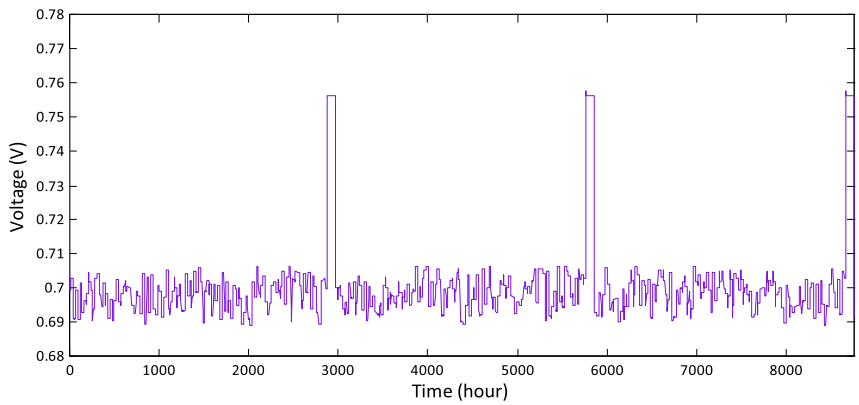

Fig. 7 – Variation in voltage according to variations in fuel supply. Increased voltage is identified during maintenance periods where fuel comes solely from hydrogen storage.

ceramic filter the gas is injected with sodium bicarbonate which converts the HCl and SO_2 to valuable NaCl (table salt) and Na_2SO_4 (detergent filler material). The solid materials are removed from the gas where the salts can be extracted and sold.

Results from the high and low temperature shift reactions show a 30% increase in H_2 as a result of the high temperature shift reactor, and a 55% increase in H_2 from the low temperature shift thereby providing an overall increase of 103%.

From the low temperature shift the gas is then compressed and cooled in preparation for desulphurisation. The Selexol™ adsorbent then extracts H_2S, COS, CO_2, N_2 and a small amount of H_2 at high pressure (40 bar) and near ambient temperature in a 20 stage distillation column. The rich Selexol™ is then pumped to a secondary 6 stage distillation column that includes a condenser and reboiler. Before entering the secondary column the pressure of the Selexol™ is dropped to 6.9 bar and heated to 125 °C. The column itself operates at ambient pressure and the distillate temperature for condensing is 100 °C and the reboiler recycles the now lean Selexol™ from the bottom of the column at 150 °C. Before being recycled back to the first column the Selexol™ must be cooled to −6 °C. Much of this is done by heating the purified syngas as it leaves the first column as the gas experiences a drop in temperature when expanding from 40 bar to ambient pressure. The remaining cooling is carried out through a refrigeration cycle which will add to the parasitic load.

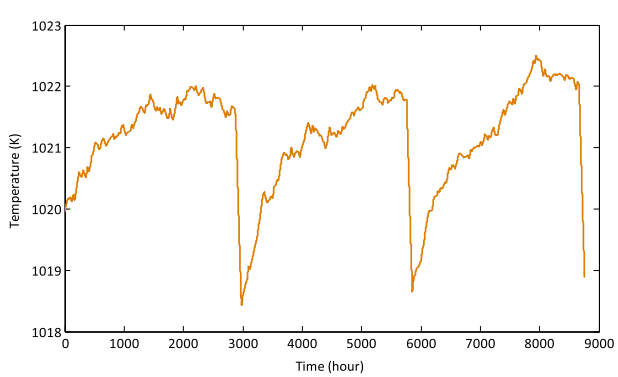

Fig. 8 – Cell temperature as a function of the annual syngas fluctuations whilst using an inlet temperature of 760 °C.

Table 6 – SOFC characteristics and variables.

Cell geometry		
Layer thicknesses		
Anode	0.0005	m
Electrolyte	0.00003	m
Cathode	0.00003	m
Planar dimensions		
Cell area	0.01	m^2
Total no. of cells	1,764,177,570	
Nusselt geometry ratio	1	
Hydraulic diameter (*Hd*)	0.005	
Material properties		
Densities		
Anode	6200	kg/m^3
Electrolyte	5560	kg/m^3
Cathode	6000	kg/m^3
Interconnects	7700	kg/m^3
Specific heats (C_p)		
Anode	650	J/kg.K
Electrolyte	300	J/kg.K
Cathode	900	J/kg.K
Interconnects	800	J/kg.K
Electrolyte conductivity (σ)	0.65	1/ohm.cm
Diffusion		
Porosity – anode (ξ)	0.35	
Porosity – cathode (ξ)	0.35	
Tortuosity – anode (τ)	4.5	
Tortuosity – cathode (τ)	4.5	
Pore radius – anode (r_e)	9.60E-07	m
Pore radius – cathode (r_e)	9.60E-07	m
Exchange current density		
Pre-exponential factor – anode (γ)	5.50E+08	A/m^2
Pre-exponential factor – cathode (γ)	7.00E+08	
Activation energy – anode (E_{act})	100,000	J/mol
Activation energy – cathode (E_{act})	120,000	J/mol
Electron transfer coefficient – anode (α)	0.5	
Electron transfer coefficient – cathode (α)	0.5	

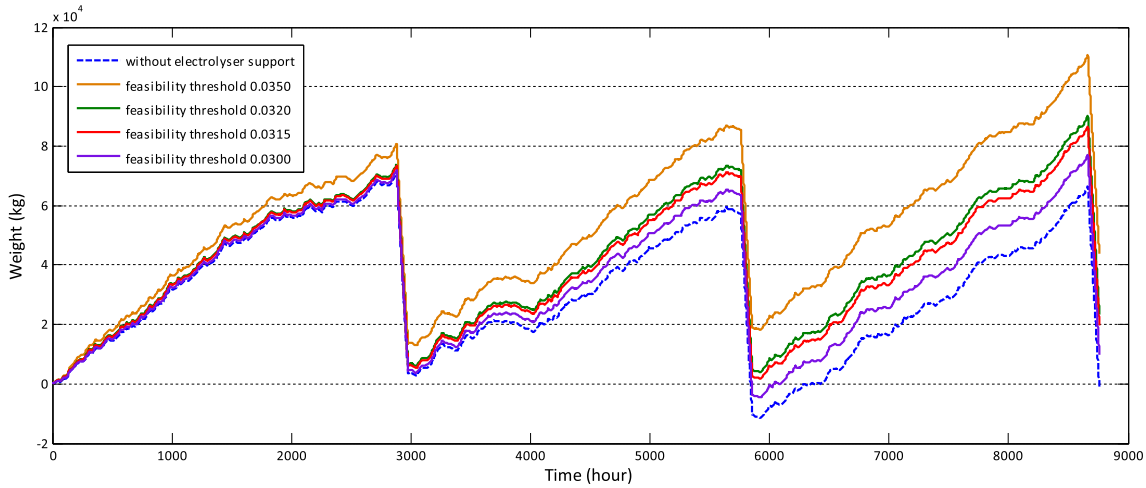

Fig. 9 – Meeting annual hydrogen demand by changes to feasibility threshold showing for the given upper and lower hydrogen limits a feasibility threshold of 0.0315 £/kWh.

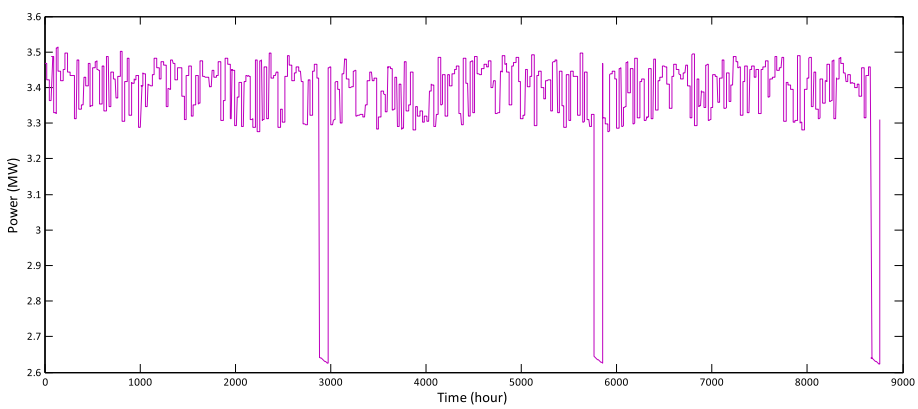

Fig. 10 – Power fluctuations according to changes in fuel composition to the burner and heat used to drive the hydrogen storage during scheduled maintenance.

Table 4 provides a complete breakdown of contaminants and the level of purification achieved, and Table 5 shows a full list of inputs and outputs from the ChemCad model.

SOFC

Using the mathematical descriptors j-V and efficiency curves have been generated to describe the overall performance of the fuel cell according to the annual fluctuations in the fuel supply and a hydrogen flow rate – between 702 and 707 kg/h.

The variation in electrical efficiency fluctuates according the flow of hydrogen to the fuel cell and benefits when the fuel cell is supplied with pure hydrogen over the maintenance periods showing spikes above 55%. The efficiency curves follow the same pattern shown in the output cell voltage presented in Fig. 7.

Fig. 8 shows that by applying an inlet temperature of 760 °C and by using the annual variation of the syngas composition the fuel cell will continue to operate close to its designated 850 °C. Fig. 8 also shows sharp drops in temperature as the fuel composition changes during the scheduled maintenance periods. A full list model assumptions are provided in Table 6.

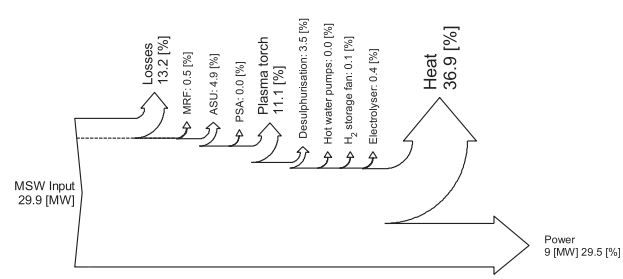

Fig. 11 – Sankey diagram showing losses and outputs.

Hydrogen production and storage

There are important aspects to consider when implementing hydrogen storage especially when scaled to cover the maintenance period of such a large system. Hydrogen is collected from excess coming from fluctuations in the syngas and from an electrolyser whose operation is controlled by the feasibility of the wholesale electricity price. This means the accumulation of hydrogen is determined by; the upper and lower hydrogen tolerance limits, feasibility threshold, and size of electrolyser. Fig. 9 shows the accumulation of hydrogen when relying purely on hydrogen from the syngas. Fig. 9 shows the hourly flow rate of hydrogen coming from the electrolyser sized at 1.2 MW. In this scenario it is important to keep the feasibility ratio as low as possible as the hydrogen produced by the electrolyser includes losses from the fuel cell, electrolyser and eventually the hydrogen storage unit when considering the initial hydrogen coming from the syngas. This will become less of an issue as more renewable energy comes on line and the spot price of electricity comes down during periods where grid flexibility is required. This could be made easier by directly connecting these renewables to WHHE Energy Centres.

Heat engine

The gas turbine operates with a pressure of 10 bar with heat coming from the fuel cell and oxy combustor. The compressor and expander have simulated with isentropic efficiencies of 85% and 86% respectively. During the scheduled maintenance periods the priority is to ensure the fuel cell remains operational meaning the heat required by the hydrogen storage becomes of greater importance. This means during these periods heat from the burner could be diverted to the hydrogen storage before entering the GT heat exchanger thereby affecting performance as shown in Fig. 10.

Overall performance

The parasitic load for the WHHE Energy Centre include; material recovery facility, air separation unit, plasma torch, the desulphurisation circuit (compressor, pumps, refrigeration), hot water pumps, hydrogen storage cooling fans, and the electrolyser. The material recovery facility is assumed to consume 20 kWh/tonne [31,32].

The average annual output and demand of the various components are shown in Fig. 11.

The annual performance of the plant shows good electrical efficiencies hovering below 30% (including the material recovery facility) which is above the industry target of 25%. During the scheduled maintenance period the parasitic losses associated with the operation of the gasifier falls away and explains the improved values shown in Fig. 12.Due to the high demand for heat from the hydrogen storage unit and because of the lack of heat coming from the gasifier over the maintenance periods the heat and combined heat and power (CHP) efficiencies see drops in values (Fig. 12).

Conclusions

Conclusions from these results show that the WHHE Energy can offer considerable advancement of WtE systems by offering:

- Improved overall electrical efficiency of 29.5% which surpasses the industry target of 25% (including material recovery facility energy demands).
- Controlled emissions and plant designs that preclude the need for tall ventilation stacks would make these systems better suited for more central locations where intelligent heat networks can be utilised.
- The ability to export heat as CHP plant would increase the combined efficiency to 66.4%.
- Employing high temperature plasma, whilst drawing considerable energy that penalises output efficiencies, means the WHHE Energy Centre can produce a high quality syngas (with fewer impurities) and can handle almost any waste grade/type.
- WHHE Energy Centres will not only serve to reduce the need for landfill but can also be used to mine landfill sites containing extremely large amounts of stored waste.

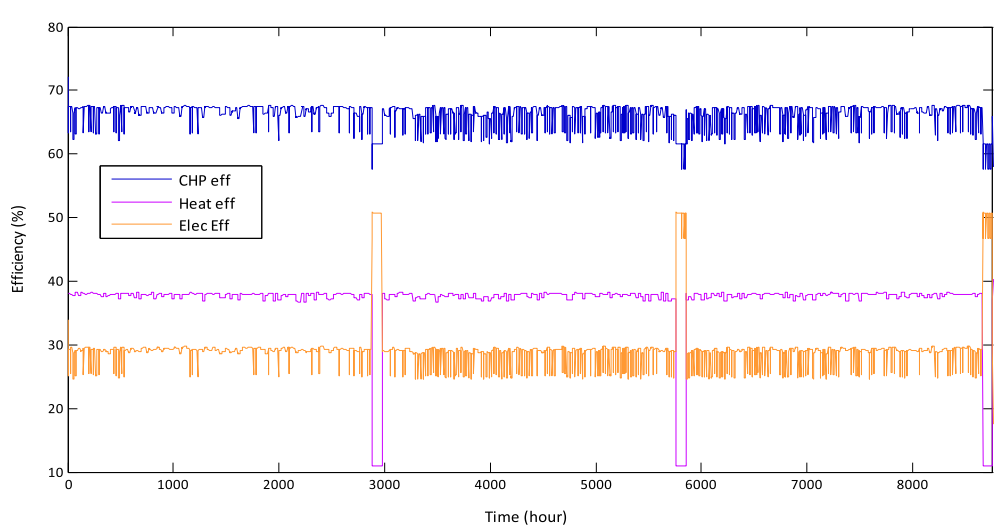

Fig. 12 – Annual electrical, heat and CHP efficiencies.

Allowing land to be reclaimed and protected against future deposits.

- An onsite hydrogen refuelling station would facilitate the much needed decarbonizing of the transport sector.
- Hydrogen production through electrolysis does not offer an immediate benefit using historical wholesale electricity prices but if connected directly with renewables or when renewables begin to have a bigger impact on wholesale prices the inclusion of an electrolyser will support both the financial and energy storage targets.

Acknowledgements

This work was made possible through the sponsorship and support of ChapmanBDSP and the Engineering and Physical Sciences Research Council in the UK.

Nomenclature

A	area (m^2)
act	activation
ASR	area specific resistance
CCE	carbon conversion efficiency (%)
c	concentration (mol/m^3)
c_p	specific heat capacity (kJ/kmol.K)
D	diffusivity (m^2/s)
E	electrical potential difference (V)
ECE	energy conversion efficiency (%)
F	Faraday's constant (C/mol)
f_1	parameter related to Faraday efficiency (mA^2/cm^4)
f_2	parameter related to Faraday efficiency (–)
G	Gibbs free energy (kJ, kJ/mol)
i	current (A)
j	Current density (A/m^2)
K	equilibrium constant (–)
m	mass (kg)
$\dot{n}$	molar flow rate (mol/s)
n	number of moles (mol)
p	partial pressure (kPa)
P	total pressure (kPa)
q	energy (J)
R	Universal gas constant (J/molK)
SB	steam to biomass ratio (–)
SB*	modified steam-to-biomass ratio (–)
T	temperature (K)
t	thickness (m), time
W	work (J)
z	valence number (–)
λ	stoichiometric oxygen ratio (–)
α	charge transfer coefficient (–)
γ	pre-exponential factor (A/m^2)
η	Voltage (V)
σ	characteristic length (Å); conductivity (1/Ω.cm)

Subscripts/Superscript

0	reference point
a, c	anode, cathode
act	activation
C	cold
ch	channel
chem	chemical
conc	concentration
conv	convection
e	equilibrium
eff	effective
elec	electrical
F	Faraday
f	forward
gen	generation
H	Hot
i, j	component species i, j
k	Knudsen
L	limit
M	molecular
P	product; pressure
R	reactant
r	reverse
rad	radiation
ref	reference
rev	reversible
rxn	reaction
T	temperature dependant

REFERENCES

[1] Doyle T, Dehouche Z, Aravind PV, Liu M, Stankovic S. Investigating the impact and reaction pathway of toluene on a SOFC running on syngas. Int J Hydrog Energy 2014;39:12083–91.

[2] WEC. 2013 World energy issues monitor. World Energy Council; 2013, ISBN 978 0 946121 20 5. Sourced online via: http://www.worldenergy.org/publications/.

[3] Shafiee S, Topal E. When will fossil fuel reserves be diminished? Energy Policy 2009;37:181–9.

[4] Sinden G. Wind power and the UK wind resource. Environmental Change Institute, University of Oxford; 2005. 2005.

[5] Eurostat. Municipal waste generation and treatment, by type of treatment method. 2009. Sourced online via: http://epp.eurostat.ec.europa.eu/portal/page/portal/waste/key_waste_streams/municipal_waste.

[6] Dohogne J. Inventory of good practices regarding (bio)-waste minimization in Europe. Miniwaste.eu; 2014. Sourced online at: http://www.miniwaste.eu/mediastore/fckEditor/file/Miniwaste_good_practices_inventory.pdf.

[7] Europa. Brochure – being wise with waste: the EU's approach to waste management. Luxembourg: European Union; 2010. 2010. Sourced online at: http://ec.europa.eu/environment/waste/pdf/WASTE%20BROCHURE.pdf.

[8] Nehrir MH, Wang C. Modeling and control of fuel cells: distributed generation applications. Wiley-IEEE Press; 2009. 2009.

[9] Costamagna P, Selimovic A, Del Borghi M, Agnew G. Electrochemical model of the integrated planar solid oxide fuel cell (IP-SOFC). Chem Eng J 2003;102:61–9 (2004).

[10] O'Hayre R, Cha S, Colella W, Prinz FB. Fuel cell fundamentals. 2nd ed. John Wiley & Sons; 2009.

[11] Uzunoglu M, Onar OC, Alam MS. Modeling, control and simulation of A PV/FC/UC based hybrid power generation

system for stand-alone applications. Renew Energy 2009;34:509–20.
[12] Ural Z, Gencoglu MT. Design and simulation of a solar-hydrogen system for different situations. Int J Hydrogen Energy 2013;39:8833–40 (2014).
[13] Ulleberg Ø. Modeling of advanced alkaline electrolyzers: a system simulation approach. Int J Hydrogen Energy 2003;28:21–33.
[14] de Rango P, Chaise A, Charbonnier J, Fruchart D, Jehan M, Marty Ph, et al. Nanostructured magnesium hydride for pilot tank development. J Alloys Compd 2007;446–447:52–7.
[15] Dornheim M. Thermodynamics of Metal Hydrides: Tailoring Reaction Enthalpies of Hydrogen Storage Materials. In: Moreno Pirajan Juan Carlos, editor. Thermodynamics – interaction studies – solids, liquids and gases. InTech; 2011.
[16] Zhong HC, Wang H, Liu JW, Sun DL, Zhu M. Altered desorption enthalpy of MgH_2 by the reversible formation of Mg(In) solid solution. Scr Mater 2011;65:285–7.
[17] Dehouche Z, Peretti HA, Hamoudi S, Yoo Y, Belkacemi K. Effect of activated alloys on hydrogen discharge kinetics of MgH_2 nanocrystals. J Alloys Compd 2008;455(1–2):432–9.
[18] McAllister S, Chen J, Fernandez-Pello AC. Fundamentals of combustion processes. Springer; 2011 [Chapter 2].
[19] CIWM. Energy from waste: a good practice guide. IWM Business Service Ltd., The Chartered Institution of Wastes Management; 2003.
[20] Ricketts B, Hotchkiss R, Livingston B, Hall M. Technology status review of waste/biomass co-gasification with coal. In: IChemE fifth European gasification conference, Noordwijk, The Netherlands; 2002.
[21] Optimat Ltd. Co-utilisation of coal and municipal wastes. 2001. Report No. COAL R212 DTI/Pub URN 01/1302.
[22] Ray R, Taylor R, Chapman C. The deployment of an advanced gasification technology in the treatment of household and other waste streams. Process Saf Environ Prot 2012;90:213–20.
[23] Davidson R. Experience of cofiring waste with coal. IEA Coal Research 1999; 1999, ISBN 92-9029-322-5.
[24] Chapman C, Taylor R, Ray R. The Gasplasma™ process: its application in Enhanced Landfill Mining. In: 1st international symposium on enhanced landfill mining, houthalen-helchteren, 4–6 october 2010; 2010.
[25] Siedlecki M, de Jong W, Verkooijen A. Fluidized bed gasification as a mature and reliable technology for the production of bio-syngas and applied in the production of liquid transportation fuels—a review. Energies 2011;4:389–434.
[26] Materazzi M, Lettieri P, Mazzei L, Taylor R, Chapman C. Technical Aspects and Thermodynamic Evaluation of a Two Stage Fluid Bed-Plasma Process for Solid Waste Gasification. In: ECI Symposium Series, editor. Refereed conference proceedings: the 14th internation conference on fluidization – from fundamentals to products; 2013. Volume (2013), http://dc.engconfintl.org/fluidization_xiv/13.
[27] Byun Y, Cho M, Chung JW, Namkung W, Lee HD, Jang SD, et al. Hydrogen recovery from the thermal plasma gasification of solid waste. J Hazard Mater 2011;190:317–23.
[28] EB Nationwide. Variation in the composition of household collected waste. EB Nationwide; 2004 [shanks first fund)].
[29] NWRWMG. Household waste composition analysis. NWRWMG Residual Waste Project; 2010. IBR0108/Reports.
[30] Jones A, Nesaratnam S, Porteous A. The open university household waste study: key findings from 2008. Defra; 2008. August 2008.
[31] DECCW NSW. Appendix 7 – assumption, collection, treatment, material recovery and energy assumptions, environment benefits of recycling. Sydney: Department of Environment, Climate Change and Water NSW; 2010.
[32] RMCT. Material recovery facility: handbook. Recycling marketing cooperative for Tennessee; 2003. Sourced online via: http://ctasgis02.psur.utk.edu/Environment/solid%20waste%20documents/recycling/material%20recovery%20facility%20handbook.pdf.